Journal of Applied Physics ARTICLE scitation.org/journal/jap

Impact of the p^+ layer on current-voltage characteristics of Cu(In,Ga)Se_2-based solar cells

Cite as: J. Appl. Phys. **125**, 043102 (2019); doi: 10.1063/1.5049388
Submitted: 20 July 2018 · Accepted: 9 January 2019 ·
Published Online: 25 January 2019

View Online Export Citation CrossMark

Marek Maciaszek

AFFILIATIONS

Faculty of Physics, Warsaw University of Technology, Koszykowa 75, 00-662 Warszawa, Poland

ABSTRACT

Cu(In,Ga)Se_2-based solar cells often exhibit fill factor losses at low temperature, in particular after red illumination or reverse biasing. A narrow p^+ layer between the absorber and buffer layers is commonly assumed to explain these effects. In this contribution, we analyze by means of analytical and numeric models the influence of the parameters of the p^+ layer on current-voltage characteristics. Specifically, we find expressions linking the voltage at which the deterioration of the current-voltage curve begins with the acceptor density and the width of the p^+ layer. Moreover, we derive formulas describing the height of the barrier in the conduction band caused by the p^+ layer. Examples of the analysis of simulated current-voltage characteristics using our approach are presented. Based on the voltage at which the decrease of the current starts, it is possible to estimate the upper and lower limits of the density of the acceptors in the p^+ layer. Furthermore, we analyze the relationship between the fill factor and the height of the barrier in the conduction band, which is determined by the density of acceptors in the p^+ layer.

I. INTRODUCTION

Many experimental studies of solar cells based on Cu(In,Ga)Se_2 (CIGS) suggest that properties of the absorber material significantly change in the vicinity of the interface with the buffer layer.[1–6] Although experiments involving structural methods did not solve this problem unambigously,[7] it is believed that electrical characteristics of CIGS-based solar cells cannot be explained without the assumption of a special layer between the standard CIGS and the interface CIGS/buffer. Arguments for the existence of a special layer were delivered by, e.g., current-voltage,[5] capacitance-voltage,[2] as well as electron beam induced current[6] characteristics.

Two models of a special layer have been commonly employed: the ordered-defect-compound (ODC) layer and the p^+ layer (or "acceptor rich layer"). The ODC model was proposed in Ref. 1. This model assumes a layer consisting of periodically located III_{Cu}-$2V_{Cu}$ defects. This special layer can be considered a separate phase, e.g., Cu(In,Ga)$_3$$Se_5$. It is highly resistive and its bandgap is around 1.3-1.4 eV.

The p^+ model was formulated by Niemegeers *et al.*[8] It assumes a narrow layer containing $\sim 10^{17}$ cm^{-3} acceptors. In further papers, authors considered shallow acceptors and/or deep recombination centers to explain the existence of this layer. The assumed thickness of the p^+ layer varies from 15 nm[8] to >100.[9] Further development of the p^+ layer model was based on *ab initio* calculations.[3,4,10–12] It was proposed that the source of additional charge is metastable defects (V_{Se} or In_{Cu}), which can significantly increase the density of acceptors if the Fermi energy is sufficiently high (as occurs close to the interface). Recent simulation studies support the p^+ layer model or the combination of the p^+ layer and the ODC model (i.e., high density of acceptors and increased bandgap).[5,6] Its two significant advantages are (1) a good correspondence with current-voltage characteristics and (2) a relationship with *ab initio* calculations. In the framework of the p^+ layer model, it was possible to model the unusual features of current-voltage characteristics of Cu(In,Ga)Se_2-based solar cells, like a kink at low temperatures, a cross-over of dark and light curves, and metastable changes induced by reverse-biasing.

The existence of the p^+ layer may lead to the appearance of a barrier in the conduction band ("CB bulge"). It was proposed that this barrier is a reason for the fill factor deficiencies observed during red illumination or in metastable states induced by light or reverse biasing[4,5] (Fig. 1). Figure 1(a) illustrates changes of the fill factor caused by illumination ("light-soaking," LS) in short- and open-circuit conditions at room temperature. After cooling to 120 K, the current-voltage characteristic exhibits so-called double diode behavior [Fig. 1(b)]. These observations were explained by changes of the width

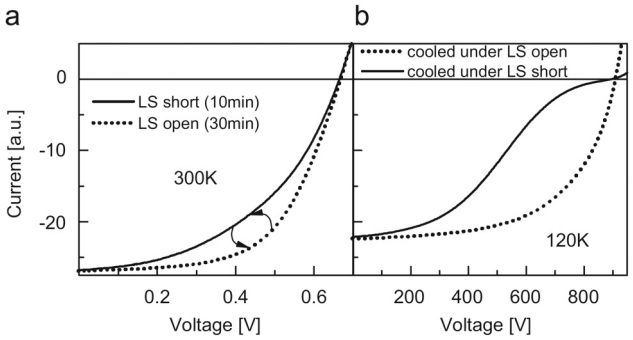

FIG. 1. Current-voltage dependences measured in the $Cu(In,Ga)Se_2$-based solar cell with a Zn(O,S) buffer layer after illumination in open- and short-circuit conditions at (a) 300 K and (b) 120 K. Reprinted with permission from Igalson *et al.*, Sol. Energy Mater. Sol. Cells **93**, 1290 (2009). Copyright 2009 Elsevier.

or doping of the p^+ layer. The value of the voltage at which the curve starts to deteriorate depends on many factors, including parameters of the structure (e.g., the width of the buffer layer[6]) and bias or light treatment. In particular, red illumination during reverse-bias treatment induces very strong deterioration of the current-voltage curve, with the decrease of the current beginning at negative voltages.[2] Although it is known that the impact of the p^+ layer is stronger when its acceptor density or width is larger, there are no systematic studies relating parameters of the p^+ layer with the barrier.

In this contribution, we focus on the quantitative analysis of the p^+ model. Our goal is to investigate the influence of properties of the p^+ layer on the fill factor of current-voltage curves. We derive relationships between characteristic features of current-voltage curves and the properties of the p^+ layer, like its thickness and density of acceptors. Presented findings could serve as a tool in the analysis of experimental results and allow for deeper insight into the properties of the CIGS in the vicinity of the interface on the basis of only electrical measurements.

In Sec. II, the rigorous analysis of the p^+ model is presented. After the explanation of the model and accepted assumptions, we look for solutions of two questions: (1) For which value of the applied voltage does there appear a barrier for electrons in the conduction band, and (2) what is the dependence of the height of the barrier on the applied voltage? Details of derivations are presented in the Appendixes. In Sec. III, the derived formulas are applied to the analysis of simulated current-voltage curves. These simulations demonstrate the impact of different parameters of the p^+ layer on the shape of the current-voltage curve. We demonstrate the advantages of our approach and point out factors that should be taken into account in analyses. The correspondence of simulations and analytical findings with experimental data is discussed. Moreover, we briefly comment on a relationship between our results and a common model explaining the existence of the p^+ layer by metastable defects. Section IV contains conclusions of the study.

II. ANALYSIS OF THE MODEL

A. Model of the structure

For the sake of simplicity, though a typical structure of the $Cu(In,Ga)Se_2$-based solar cell is more complicated, we consider a simplified structure consisting of four layers: standard $Cu(In,Ga)Se_2$, p^+ layer, buffer, and highly doped window. The "buffer" represents all the lower doped layers (as compared to the window layer) between the p^+ and window layers. In the case of $Cu(In,Ga)Se_2$/CdS/i-ZnO/ZnO:Al solar cells, the "buffer" can be understood as a sum of CdS and i-ZnO layers. To enable an analytical approach, some further simplifications are necessary.

Firstly, we assume a uniform doping of all layers. Thus, we treat defect states in the p^+ layer as shallow. We do not exclude the existence of deep recombination centers in the p^+ layer but we assume that their influence on the charge density is negligible. Secondly, we assume a low density of nonequilibrium carriers.

In our calculations, it is necessary to assume some position of the Fermi level at the p^+/buffer interface. To deal with this problem, we analyze three possible cases: highly doped buffer layer [Fermi level at the interface pinned at the conduction band minimum (CBM) of the buffer], averagely doped buffer layer (thickness of the buffer layer wider than the depletion width), and lowly doped buffer layer (buffer layer depleted in its whole thickness). In all analyses, high doping of the window layer (effective density of states in the conduction band equal to the donor density) was assumed. Examples of buffer layers representing analyzed cases are mentioned in Sec. II D.

We do not consider a conduction band offset at the p^+/buffer interface, deep acceptors in the buffer layer, a barrier at the buffer/window interface, nor other phenomena which may have influence on the potential distribution in the structure. It should be stressed that our goal is not to refine simulation models but to treat analytically the well known p^+ model in its simplified version. Hence, a perfect accordance between current-voltage curves simulated in this contribution and experimental ones is not the main goal. On the other hand, the impact of the position of the valence band maximum (VBM) in the p^+ layer will be analyzed. The valence band offset will be denoted as ΔE_V.

Figure 2 shows a scheme of the analyzed structure. As a point "0," we assume the edge of the space charge region in CIGS. x_{CIGS} is the width of the space charge region in the standard CIGS, and N_{CIGS} is the acceptor density in the standard CIGS. x_{p+} is the thickness of the p^+ layer, and N_{p+} stands for the acceptor density in the p^+ layer. By N_{buf} and x_{buf}, we denote parameters of the buffer layer: the donor density and the thickness, respectively. x_{bSCR} is a width of the space charge region in the buffer layer.

B. Effect of the p^+ layer on the band diagram

To present the influence of the p^+ layer on the band diagram, we show results of simulations obtained for two

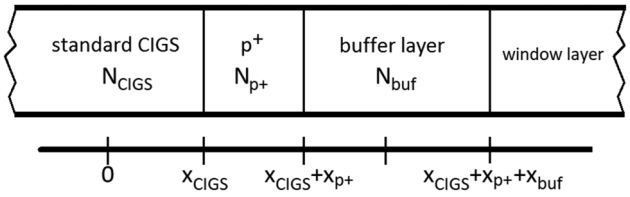

FIG. 2. Scheme of the analyzed structure. The point marked inside the buffer layer is the edge of the space charge region. If this point lies inside the buffer (the case of the averagely doped buffer layer), its position is $x_{CIGS} + x_{p+} + x_{bSCR}$.

different values of the applied voltage V_{dc}. Diagrams were obtained using SCAPS software.[13] Figure 3(a) shows the energy of the conduction band minimum (CBM) obtained for two values of the applied voltage V_{dc}: 0 and 0.5 V (assumed parameters: $N_{CIGS} = 3 \times 10^{15}\,cm^{-3}$, $N_{p+} = 3 \times 10^{17}\,cm^{-3}$, $x_{p+} = 50\,nm$, $N_{buf} = 10^{18}\,cm^{-3}$). In the case of $V_{dc} = 0.5\,V$, a

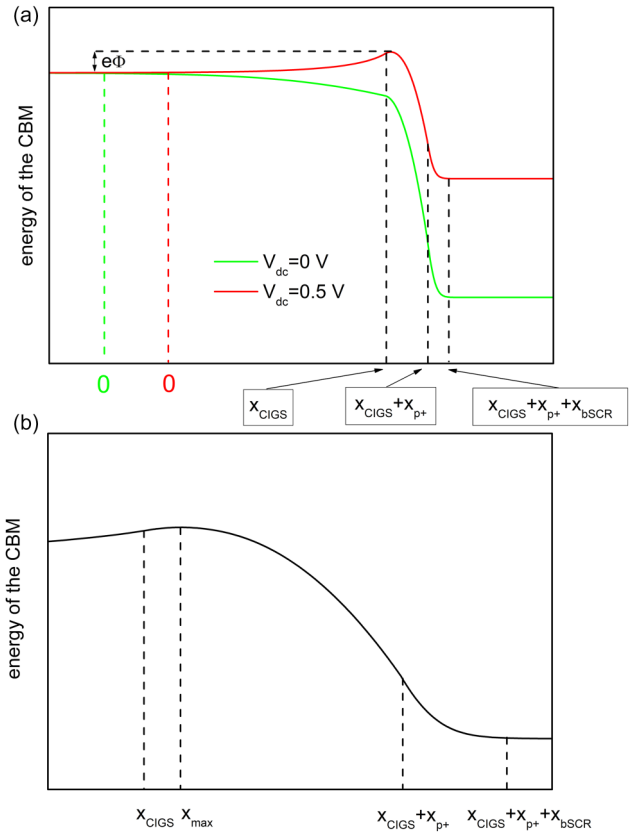

FIG. 3. (a) The energy of the CBM in the structure for two values of V_{dc}: 0 and 0.5 V. In the case of 0.5 V, a barrier of height Φ is visible. The width of the space charge region depends on the applied voltage; thus, the position of "0" is different for 0 and 0.5 V (a small difference in x_{bSCR} is neglected). (b) The energy of the CBM in the p^+ layer in the presence of the barrier Φ.

barrier in the conduction band is visible. Its height is denoted by Φ. In Fig. 3(b), we show the energy of the CBM in the p^+ layer [a magnification of Fig. 3(a)]. It should be noticed that the maximal height of the barrier does not correspond to $x = x_{CIGS}$. By x_{max}, we denote a position corresponding to the maximal height of the barrier. The difference between x_{CIGS} and x_{max} is particularly influential in the case of larger Φ.

C. Analytical approach

Dependences of the current density j on the applied voltage V_{dc} of structures with the p^+ layer exhibit a double diode behavior, also called a kink [Fig. 1(b)]. The value of V_{dc}, at which the $j(V_{dc})$ curve starts to deteriorate, is denoted by V_{kink}. As a quantitative definition of V_{kink}, it can be proposed that $j(V_{kink}) = 0.95 \times j(V_{dc} \ll V_{kink})$, i.e., 95% of the current corresponding to the flat part of the curve (which is equal to j_{sc} in the case of kinks occurring at positive voltages). For $V_{dc} > V_{kink}$, the current is decreased by the barrier in the CBM.

By means of the analytical approach, we solve two problems: (1) how V_{kink} depends on parameters of the p^+ layer and (2) how the height of the barrier Φ depends on V_{dc}. To achieve this objective, we solve the Poisson equation. By p, E_F, E_{Fp}, and E_V we denote the density of holes, the Fermi energy, the hole quasi-Fermi energy, and the energy of the valence band maximum (VBM), respectively.

If the barrier exists ($\Phi > 0$), energy bands in the standard CIGS (between 0 and x_{CIGS}) rise (cf. Fig. 3). As a result, energy of the VBM is closer to the Fermi energy (or the hole quasi-Fermi energy) between 0 and x_{CIGS} than in the bulk ($x < 0$). In this region, holes have a larger contribution to the electrical charge than acceptors ($p > N_{CIGS}$). Hence, it is necessary to take into account not only the charge introduced by acceptors (eN_{CIGS}) but also by holes (ep).

It is noteworthy that for large widths of the p^+ layer (x_{p+}), the analyzed structure can be considered two junctions: CIGS/p^+ (which is the isotype one) and p^+/buffer. In other words, a neutral region between these two junctions appears. For typical values of x_{p+}, the structure is an intermediate case between one junction (CIGS/buffer; $x_{p+} = 0$) and two junctions (large x_{p+}). It can be seen from this that the maximal position of the Fermi level (achieved for sufficiently large x_{p+}) in the p^+ layer corresponds to $p = N_{p+}$. Thus, it is clear that in the p^+ layer, the acceptor density (N_{p+}) is larger (in the extreme case: equal) than the hole concentration (p).

If the height of the barrier is large, the distance between E_V and E_{Fp} is small. The smallest value of $E_{Fp} - E_V$ corresponds to $x = x_{max}$. As a consequence, it is possible that p in the p^+ layer has a significant influence on the total charge. For the sake of accuracy, we should also take into account p in the p^+ layer when the barrier exists.

With all the discussed assumptions, Poisson's equations describing the considered structure are

$$\frac{d^2\varphi}{dx^2} = \frac{eN_{CIGS} - ep}{\varepsilon_0\varepsilon_1} \quad \text{for } 0 < x < x_{CIGS}, \tag{1a}$$

$$\frac{d^2\varphi}{dx^2} = \frac{eN_{p+} - ep}{\varepsilon_0\varepsilon_1} \quad \text{for } x_{CIGS} < x < x_{CIGS} + x_{p+}, \tag{1b}$$

$$\frac{d^2\varphi}{dx^2} = \frac{-eN_{buf}}{\varepsilon_0\varepsilon_2} \quad \text{for } x_{CIGS} + x_{p+} < x < x_{CIGS} + x_{p+} + x_{bSCR}, \tag{1c}$$

where φ stands for the electric potential (should not be confused with Φ, which is the height of the barrier). ϵ_1 is a dielectric constant of Cu(In,Ga)Se_2, and ϵ_2 is a dielectric constant of the buffer layer.

Our approach is based on the fact that the barrier in energy bands is a minimum of the electric potential. The barrier exists, if at some point ($x = x_{max}$) inside the junction the electric potential achieves minimum. In this point, the electric field is zero.

The final formulas should include only N_{CIGS}, N_{p+}, N_{buf}, x_{p+}, x_{buf}, and dielectric constants. They should not include x_{CIGS} or x_{bSCR} because the experimental determination of their values is not straightforward.

D. How V_{kink} depends on parameters of the p^+ layer?

Details of the derivation can be found in Appendix A. Here, we present only its results. In our analysis, three cases are considered:

(a) highly doped buffer (depletion width in the buffer layer negligible; Fermi level achieves the CBM at the p^+/buffer interface),
(b) averagely doped buffer layer (depletion width narrower than the thickness of the buffer layer), and
(c) lowly doped buffer layer (buffer layer depleted in its whole thickness; highly doped window layer; Fermi level pinned at the buffer/window interface).

They correspond to three cases shown in Fig. 4: black ($N_{buf} = 5\times10^{18}$ cm^{-3}), red ($N_{buf} = 5\times10^{17}$ cm^{-3}), and green line ($N_{buf} = 5\times10^{16}$ cm^{-3}) represent highly, averagely, and lowly doped buffer layers, respectively.

It can be supposed that solar cells with $Zn_{1-x}Mg_xO$ buffer layers (usually highly doped[14]) or without buffer layers[15] quite well correspond to case a, whereas structures with CdS buffer layers represent case c.

If N_{buf} is high (case a), bands in the buffer layer can be assumed flat, and the Fermi level approaches the CBM at the p^+/buffer interface. Hence,

$$V_{kink} = V_{bi} - \frac{eN_{p+}x_{p+}^2}{2\varepsilon_0\varepsilon_1}, \tag{2}$$

where V_{bi} is a built-in potential, which is a potential difference between neutral regions at p and n sides (i.e., between the window layer and the neutral region of CIGS).

In the case of average N_{buf} (case b), the depletion width in the buffer layer is nonnegligible, but lower than the width of the layer. In this situation,

$$V_{kink} = V_{bi} - \frac{eN_{p+}x_{p+}^2}{2\varepsilon_0}\left(\frac{1}{\varepsilon_1} + \frac{N_{p+}}{N_{buf}\varepsilon_2}\right). \tag{3}$$

If N_{buf} is small (case c), the buffer layer is depleted in its whole thickness. It leads to

$$V_{kink} = V_{bi} - \frac{eN_{p+}x_{p+}^2}{2\varepsilon_0\varepsilon_1} - \frac{eN_{p+}x_{p+}x_{buf}}{\varepsilon_0\varepsilon_2} + \frac{eN_{buf}x_{buf}^2}{2\varepsilon_0\varepsilon_2}. \tag{4}$$

Figure 5 shows the dependence of V_{kink} of x_{p+} for cases a-c calculated using Eqs. (2)–(4). The built-in potential was

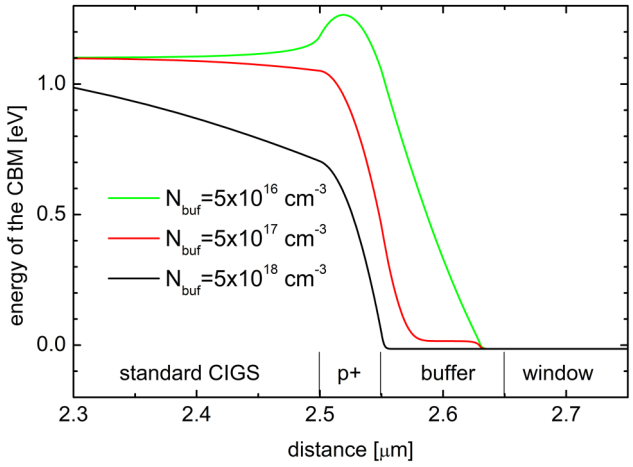

FIG. 4. The energy of the CBM in the structure for different N_{buf} and $V_{dc} = 0$.

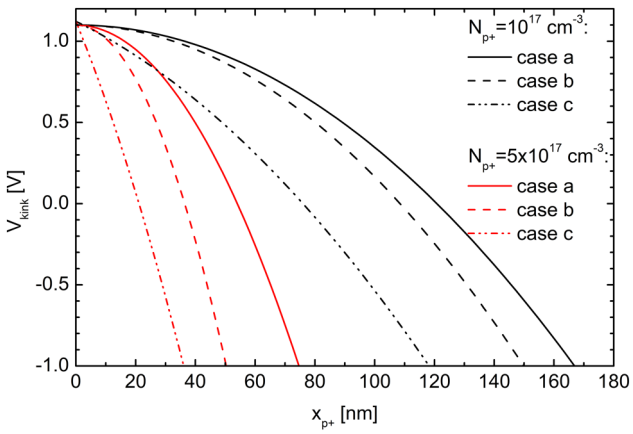

FIG. 5. V_{kink} as a function of the width of the p^+ layer (x_{p+}) in cases of highly (a), averagely (b), and lowly (c) doped buffer layer. Black and red lines represent the results obtained for N_{p+} equal to 10^{17} cm^{-3} and 5×10^{17} cm^{-3}, respectively. In cases b and c, N_{buf} was assumed equal to 5×10^{17} cm^{-3} and 10^{16} cm^{-3}, respectively.

estimated using

$$eV_{bi} = E_g - k_B T \ln \frac{N_V}{N_{CIGS}}, \quad (5)$$

where E_g is the bandgap of the standard Cu(In,Ga)Se_2. This formula is valid for cases a and c. In the case of b, this expression neglects a small difference between the Fermi energy and the energy of the CBM in the neutral region of the buffer layer. Assuming $N_{CIGS} = 3 \times 10^{15}$ cm^{-3}, T = 150 K, and $E_g = 1.2$ eV, we obtain $V_{bi} = 1.10$ V. In the case of the averagely doped buffer layer (case b), we assumed $N_{buf} = 5 \times 10^{17}$ cm^{-3}. In the case of the lowly doped buffer layer (case c), we assumed $N_{buf} = 10^{16}$ cm^{-3} and $x_{buf} = 50$ nm.

Cases b and c better correspond to the actual situation in real structures. The importance of case a comes from the fact that it leads to the simplest expression, which does not contain N_{buf} and includes only one term describing the p^+ layer: $N_{p+}x_{p+}^2$. The expression obtained in case a [Eq. (2)] can be interpreted as a higher limit of V_{kink}. V_{kink} in cases b and c is lower than in case a. Expressions for V_{kink} in cases b and c [Eqs. (3) and (4)] are more accurate but include N_{buf}, which is usually unknown. More comments on the consequences of the relationship between V_{kink} and different buffer layers can be found in Sec. III B.

In the analysis of experimental results, it is necessary to choose between Eqs. (2)–(4). Equation (2) is appropriate if $N_{buf} \gg N_{p+}$. However, a choice between Eqs. (3) and (4), corresponding to situations of completely and partially depleted buffer layer, may be not straightforward. Therefore, it is necessary to formulate a condition distinguishing between situations of completely and only partially depleted buffer layers. This condition is found in Appendix A and is based on the width of the buffer layer x_{buf}. If $N_{p+}x_{p+}/N_{buf} < x_{buf}$, Eq. (3) is adequate. Otherwise, the buffer is completely depleted, and Eq. (4) correctly describes V_{kink}.

Finally, we notice that V_{kink} does not depend on the possible valence band offset between the standard Cu(In,Ga)Se_2 and the p^+ layer.

E. How does the height of the barrier depend on the applied voltage?

Derivation of the height of the barrier is more complicated. Firstly, we present an analysis leading to the maximal height of the barrier (maximal as a function of the applied voltage). Then, we show equations relating the height of the barrier Φ with the applied voltage. As the position of the VBM determines the hole concentration, we consider two cases: with and without valence band offset between the standard Cu(In,Ga)Se_2 and the p^+ layer. Our approaches are based on searching for the minimum of the electrical potential $\varphi(x_{max})$, which occurs at the maximal height of the barrier. Since we assume $\varphi(x = 0) = 0$, Φ is equal to $-e\varphi(x_{max})$.

1. Maximal height of the barrier

As we said previously, the Cu(In,Ga)Se_2/p^+/buffer structure can be considered an intermediate case between one and two junctions. If the structure contains two junctions (CIGS/p^+ and p^+/buffer), i.e., in the p^+ layer there is a neutral region, the barrier achieves maximal height. This situation may occur if V_{dc} is sufficiently large. Further increasing of V_{dc} has no important impact on the CIGS/p^+ junction, as all the additional V_{dc} is dropped across the p^+/buffer junction.

The maximal height Φ (i.e., corresponding to sufficiently high V_{dc}) is denoted as Φ_{max}. Φ_{max} can be simply determined as the difference in the energy of the conduction band minimum between neutral regions of Cu(In,Ga)Se_2 and p^+ layer. Thus, the maximal value of Φ is

$$\Phi_{max} = \Delta E_V + k_B T \ln \frac{N_{p+}}{N_{CIGS}}. \quad (6)$$

For example, for $N_{p+} = 2 \times 10^{17}$ cm^{-3}, $N_{CIGS} = 3 \times 10^{15}$ cm^{-3}, T = 150 K, and no valence band offset ($\Delta E_V = 0$), $\Phi_{max} = 0.054$ eV.

2. No valence band offset

In the analysis of the dependence of Φ on V_{dc}, it is necessary to take into account holes in the p^+ layer. Increasing V_{dc}, the structure begins to behave as two junctions. The hole concentration at $x = x_{max}$ becomes significant. In the limiting case, a neutral region in the p^+ layer appears with $p = N_{p+}$. Neglecting p in the p^+ layer is justified only for low V_{dc}, i.e., for V_{dc} close to V_{kink}. Hence, the hole concentration in the p^+ layer can be neglected in the analysis of V_{kink} but not in the case of $\Phi(V_{dc})$.

Equations (1b) and (A2) lead to (additional details can be found in Appendix A)

$$E^2(\varphi) = \frac{2eN_{CIGS}}{\varepsilon_0 \varepsilon_1}\left[\varphi(x_{CIGS}) + \frac{k_B T}{e}\left(\exp\frac{-e\varphi}{k_B T} - 1\right)\right] + \frac{2eN_{p+}}{\varepsilon_0 \varepsilon_1}[\varphi - \varphi(x_{CIGS})]. \quad (7)$$

If the barrier exists, $E(x) > 0$ for $x_{CIGS} < x < x_{max}$ and $E(x) < 0$ for $x_{max} < x < x_{CIGS} + x_{p+}$. Taking benefit of the standard relationship between electric field and electric potential, we obtain

$$\int_{\varphi(x_{max})}^{\varphi(x_{CIGS}+x_{p+})} \frac{d\varphi}{|E(\varphi)|} + \int_{\varphi(x_{max})}^{\varphi(x_{CIGS})} \frac{d\varphi}{|E(\varphi)|} = x_{p+}, \quad (8)$$

where $|E(\varphi)|$ stands for the absolute value of the electric field found in Eq. (7).

To solve Eq. (8), it is necessary to know $\varphi(x_{CIGS} + x_{p+})$ and the relationship between $\varphi(x_{CIGS})$ and $\varphi(x_{max})$. In the case of highly doped buffer, all the potential changes between $x = 0$ and $x = x_{CIGS} + x_{p+}$. If $\varphi(x = 0) = 0$, $\varphi(x_{CIGS} + x_{p+})$ is equal to $V_{bi} - V_{dc}$. An equation linking $\varphi(x_{CIGS})$ and $\varphi(x_{max})$

can be obtained from Eq. (7) knowing that $E^2[\varphi(x_{max})] = 0$,

$$\varphi(x_{CIGS}) = \frac{N_{CIGS}k_BT}{e(N_{p+} - N_{CIGS})}\left(e^{-\frac{e\varphi(x_{max})}{k_BT}} - 1\right) + \frac{N_{p+}}{N_{p+} - N_{CIGS}}\varphi(x_{max}). \quad (9)$$

Solving Eqs. (8) and (9), $\Phi(V_{dc})$ can be calculated.

Figure 6 shows the dependence of Φ on V_{dc} for the structure with $N_{p+} = 3\times10^{17}\,cm^{-3}$, $N_{CIGS} = 3\times10^{15}\,cm^{-3}$, and highly doped buffer. Calculations were performed for different x_{p+} and temperature. In Table I, we summarized values of V_{kink} and Φ_{max} calculated using Eqs. (2) and (6), respectively. It is visible that these values correspond well to curves in Fig. 6: the barrier appears at $V_{dc} = V_{kink}$ and approaches Φ_{max} for large V_{dc}.

It is noteworthy that at higher temperatures, Φ_{max} is larger and V_{kink} is lower. As a consequence, Φ increases with the temperature. Contrary to this result, it could be supposed that in real solar cells Φ at lower temperatures (when the kink is usually observed) is equal or higher than $\Phi(T = 300\,K)$. This issue will be more deeply discussed in Sec. III.

3. Nonzero valence band offset

A lower energy of the VBM in the p^+ layer results in a lower hole concentration. Solving the Poisson equation, we derived the $E(\varphi)$ function in the case of $\Delta E_V > 0$. The equations and details of the derivation can be found in Appendix B.

Nonzero valence band offset leads to higher Φ. In the case of larger ΔE_V, the impact of holes in the p^+ layer on Φ becomes weak. In that case, it is possible to calculate Φ using simpler formulas, neglecting holes in the p^+ layer (see Appendix B). As we said previously, ΔE_V has no influence on V_{kink}.

Figure 7 shows Φ as a function of V_{dc} for different values of ΔE_V. Assumed parameters are $N_{CIGS} = 3\times10^{15}\,cm^{-3}$, $N_{p+} = 3\times10^{17}\,cm^{-3}$, $x_{p+} = 60\,nm$, and $T = 150\,K$. V_{kink} in all cases is 0.286 V. Φ_{max} for $\Delta E_V = 0$ is 0.060 eV. In other cases, it is increased by ΔE_V [cf. Eq. (6)].

TABLE I. V_{kink} and Φ_{max} calculated using Eqs. (2) and (6) for values of x_{p+} and T corresponding to $\Phi(V_{dc})$ curves shown in Fig. 6. In all cases, $N_{CIGS} = 3\times10^{15}\,cm^{-3}$, $N_{p+} = 3\times10^{17}\,cm^{-3}$, and highly doped buffer was assumed.

x_{p+} (nm)	T (K)	V_{kink} (V)	Φ_{max} (eV)
40	150	0.739	0.060
50	150	0.536	0.060
60	150	0.287	0.060
40	300	0.613	0.119
50	300	0.410	0.119
60	300	0.161	0.119

Finally, we notice that simplified equations neglecting holes in the p^+ layer [Eqs. (B5) and (B6)] give the values of Φ equal to the case of $\Delta E_V = 0.15\,eV$ in the analyzed range of V_{dc} ($0 < V_{dc} < 0.9\,V$). Formulas neglecting holes in the p^+ layer do not depend on ΔE_V. We conclude that simplified equations give a good approximation for Φ when V_{dc} is close to V_{kink}. The accuracy of this approximation rises in the case of $\Delta E_V > 0$.

III. SIMULATIONS AND DISCUSSION

In the following paragraphs, we consider impacts of different factors related to the p^+ layer on current-voltage characteristics. To highlight key phenomena and obtain more comprehensible results, we perform simulations for slightly different structures (e.g., we change the valence band offset or the width of the buffer layer).

All simulations were performed for white illumination ($1000\,W/m^2$). The bandgap of the standard $Cu(In,Ga)Se_2$

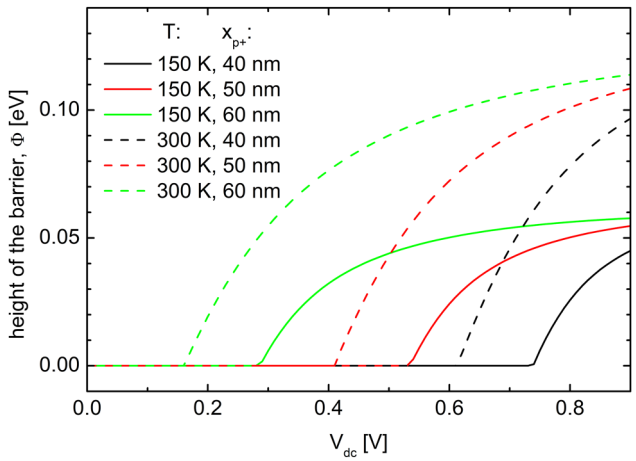

FIG. 6. The height of the barrier in the p^+ layer (Φ) as a function of the applied voltage for different temperatures and widths of the p^+ layer.

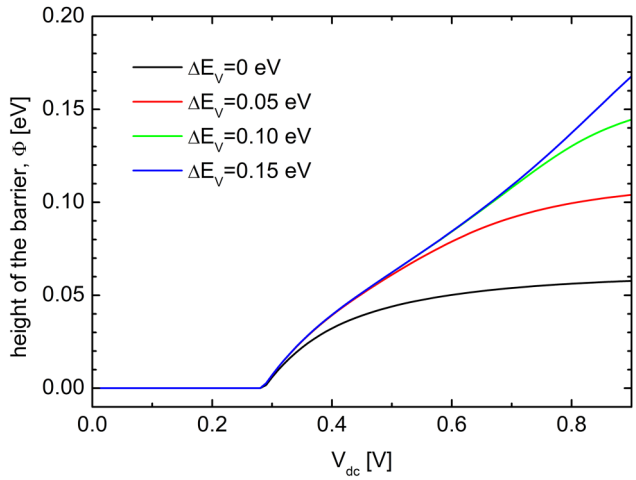

FIG. 7. The height of the barrier as a function of the applied voltage for different values of the valence band offset between the standard CIGS and the p^+ layer.

(outside the p^+ layer) is 1.2 eV and dielectric constants are equal to 12 [in standard Cu(In,Ga)Se_2 and p^+ layers] and 10 (in the buffer and window layers). The other parameters are listed in Appendix C.

A. Structures with different widths of the p^+ layer (x_{p+})

Figure 8 shows the results of simulations of $j(V_{dc})$ dependences for three different values of x_{p+}: 30 nm, 40 nm, and 50 nm. The other parameters of the structure were $N_{CIGS} = 3 \times 10^{15}\,cm^{-3}$, $N_{p+} = 3 \times 10^{17}\,cm^{-3}$, $N_{buf} = 10^{17}\,cm^{-3}$, and $x_{buf} = 100$ nm. The doping of the window layer was equal to $10^{18}\,cm^{-3}$. Simulations were performed at $T = 150$ K. The valence band offset of $\Delta E_V = 0.15$ eV was assumed (i.e., bandgaps of the standard CIGS and p^+ layer were 1.2 eV and 1.35 eV, respectively).

It is clear that V_{kink} decreases with x_{p+}. In other words, larger x_{p+} leads to stronger deterioration of the $j(V_{dc})$ curve. In order to apply the approach introduced in Sec. II, we first pay attention to the doping of the buffer layer. In the cases of widths of the p^+ layer (x_{p+}) equal to 40 nm and 50 nm, $N_{p+}x_{p+} > N_{buf}x_{buf}$. Therefore, for $V_{dc} = V_{kink}$, the buffer layer is depleted in its whole thickness (case of lowly doped buffer in Sec. II), and the adequate formula describing V_{kink} is Eq. (4). Application of this equation results in V_{kink} equal to −0.53 V and −1.27 V for $x_{p+} = 40$ nm and $x_{p+} = 50$ nm, respectively. Regarding results for $x_{p+} = 30$ nm, the depletion width in the buffer layer corresponding to $V_{dc} = V_{kink}$ is lower than the thickness of the buffer layer as $N_{buf}x_{buf} > N_{p+}x_{p+}$ (case of averagely doped buffer). Hence, Eq. (3) should be applied; it gives $V_{kink} = 0.16$ V. Calculated values of V_{kink} are marked in Fig. 8 with arrows. These values correspond well with the beginning of the decrease of the current density.

It is noteworthy that our model is sufficient to observe a decrease of the current density related to the p^+ layer and find the most important factors determining this phenomenon. However, these simulations exhibit some discrepancies with typical experimental results. In particular, we do not observe the fall of the current density to zero. In our model, electrons excited in the p^+ layer for $x_{max} < x < x_{CIGS} + x_{p+}$ are collected and are the reason for nonzero current density above V_{kink}. To correctly model this phenomenon, additional elements (like recombination centers in the p^+ layer or at interfaces) should be introduced into the model. An analytical approach in the case of a more sophisticated model would be much more difficult, however.

B. Structures with different donor densities in the buffer layer (N_{buf})

Figure 9 shows $j(V_{dc})$ characteristics simulated for three values of the donor density in the buffer layer (N_{buf}): $5 \times 10^{16}\,cm^{-3}$, $5 \times 10^{17}\,cm^{-3}$, and $5 \times 10^{18}\,cm^{-3}$. The other parameters were $T = 150$ K, $N_{CIGS} = 3 \times 10^{15}\,cm^{-3}$, $N_{p+} = 3 \times 10^{17}\,cm^{-3}$, $x_{p+} = 50$ nm, $x_{buf} = 80$ nm, and $\Delta E_V = 0.15$ eV (i.e., bandgaps of the standard CIGS and p^+ layer were 1.2 eV and 1.35 eV, respectively).

V_{kink} visibly changes with N_{buf}. In the case of high N_{buf} ($5 \times 10^{18}\,cm^{-3}$), V_{kink} is the highest and the $j(V_{dc})$ curve is less affected by the p^+ layer. Lower values of N_{buf} lead to lower V_{kink} and stronger deterioration of $j(V_{dc})$ dependence. Clearly, the same p^+ layer may result in different V_{kink}, if the distribution of the electric potential in the buffer layer is different.

Results shown in Fig. 9 represent three investigated regimes: high, average, and low doping of the buffer layer (cf. Fig. 4). In the case of $N_{buf} = 5 \times 10^{18}\,cm^{-3}$, the bands in the buffer layer can be considered flat and V_{kink} is possible to calculate via Eq. (2). To analyze the other cases, Eq. (3)

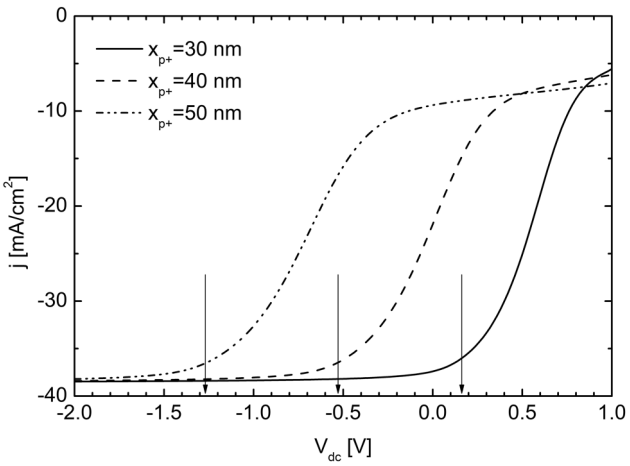

FIG. 8. $j(V_{dc})$ dependences for different widths of the p^+ layer (x_{p+}). The other parameters are $T = 150$ K, $N_{p+} = 3 \times 10^{17}\,cm^{-3}$, and $\Delta E_V = 0.15$ eV. The values of V_{kink} calculated with Eqs. (3) and (4) are marked with arrows.

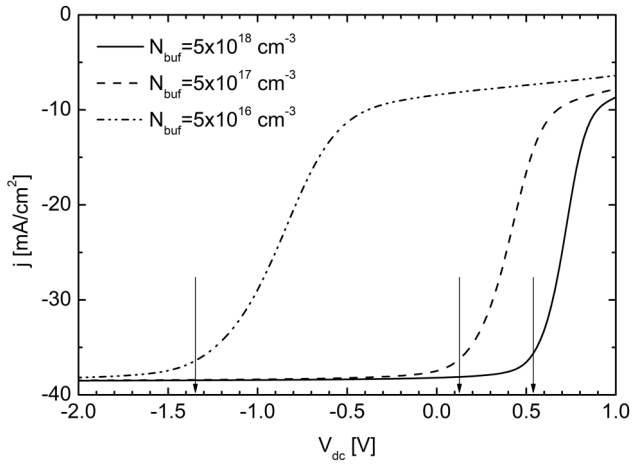

FIG. 9. $j(V_{dc})$ dependences for different values of the donor density in the buffer layer (N_{buf}). The other parameters are $T = 150$ K, $N_{p+} = 3 \times 10^{17}\,cm^{-3}$, $x_{p+} = 50$ nm, and $\Delta E_V = 0.15$ eV. The values of V_{kink} calculated with Eqs. (2)–(4) are marked with arrows.

(for $N_{buf} = 5 \times 10^{17}\,cm^{-3}$) and Eq. (4) (for $N_{buf} = 5 \times 10^{16}\,cm^{-3}$) should be used. The obtained values of V_{kink} are 0.54 V, 0.13 V, and −1.35 V for N_{buf} equal to $5 \times 10^{18}\,cm^{-3}$, $5 \times 10^{17}\,cm^{-3}$, and $5 \times 10^{16}\,cm^{-3}$, respectively.

The importance of Eqs. (2)–(4) comes from the fact that they allow for the estimation of N_{p+} and x_{p+} based on measured V_{kink}. However, N_{buf} is usually unknown and the choice of the correct formula may be difficult. We advise using Eq. (2), neglecting the impact of the buffer layer, as a first approximation. Using this formula, it is possible to calculate $N_{p+}x_{p+}^2$ which is an upper limit of the correct value. Doing the next step requires x_{p+} and x_{buf}. x_{buf} is usually known and x_{p+} may be estimated from C-V measurements. Then, a lower limit of N_{p+} can be obtained using Eq. (4) and assuming $N_{buf} = 0$ (neglecting the last term).

As an example of such approximations, we use the $j(V_{dc})$ dependence shown in Fig. 9 for $N_{buf} = 5 \times 10^{17}\,cm^{-3}$, exhibiting $V_{kink} = 0.13$ V. Knowing V_{bi} [cf. Eq. (5)] and using Eq. (2), an upper limit of $N_{p+}x_{p+}^2$ is obtained. It equals $1.29 \times 10^{7}\,cm^{-1}$. If the value of the width of the p^+ layer (x_{p+}) is known (50 nm), the upper limit of the acceptor density in the p^+ layer (N_{p+}) is $5.1 \times 10^{17}\,cm^{-3}$. The lower limit is determined through Eq. (4) with $N_{buf} = 0$. It equals to $1.1 \times 10^{17}\,cm^{-3}$. The real value of N_{p+} was $3 \times 10^{17}\,cm^{-3}$ and it is close to the middle of the determined range.

Lower doping of the buffer layer results in lower V_{kink}. This conclusion is in accordance with experiments,[3] in which stronger deterioration of the $j(V_{dc})$ curve and double diode behavior is typical rather for more resistive CdS than for more conductive $Zn_xMg_{1-x}O$ buffer layers. Moreover, if the buffer layer is lowly doped (resistive), large x_{buf} should lead to lower V_{kink} [cf. Eq. (4)]. This dependence was experimentally observed in Ref. 6 for CdS buffer layers in the wide range of x_{buf} (from 25 to 170 nm).

C. Structures with different parameters of the p^+ layer (N_{p+} and x_{p+}) but equal V_{kink}

V_{kink} has a clear impact on the fill factor. One value of V_{kink} corresponds to many combinations of N_{p+} and x_{p+}, however. Comparing $j(V_{dc})$ dependences for different parameters of the p^+ layer but exhibiting equal V_{kink} enables us to distinguish impacts of N_{p+} and x_{p+} on the fill factor. We consider structures with $N_{CIGS} = 3 \times 10^{15}\,cm^{-3}$, a highly doped buffer ($N_{buf} = 5 \times 10^{19}\,cm^{-3}$), and different pairs of N_{p+} (ranging from $5 \times 10^{16}\,cm^{-3}$ to $5 \times 10^{17}\,cm^{-3}$) and x_{p+} (Fig. 10). Simulations were performed at T = 150 K. No ΔE_V was assumed.

All curves exhibit V_{kink} equal to 0.2 V. The values of x_{p+} for given N_{p+} resulting in assumed V_{kink} can be found by a trial and error approach, but we used a formula linking V_{kink}, N_{p+}, and x_{p+} derived in Sec. II [Eq. (2)]. It was necessary to assume quite large x_{p+} to obtain $V_{kink} = 0.2$ V (cf. Fig. 8, where $V_{kink} = 0.16$ V was obtained for $x_{p+} = 30$ nm and $N_{p+} = 3 \times 10^{17}\,cm^{-3}$ but lower doping of the buffer layer).

It is visible that in the case of equal V_{kink}, structures with higher N_{p+} exhibit lower FF. In the case of $N_{p+} = 5 \times 10^{17}\,cm^{-3}$ and $x_{p+} = 49$ nm (a magenta line in Fig. 10), FF = 52%.

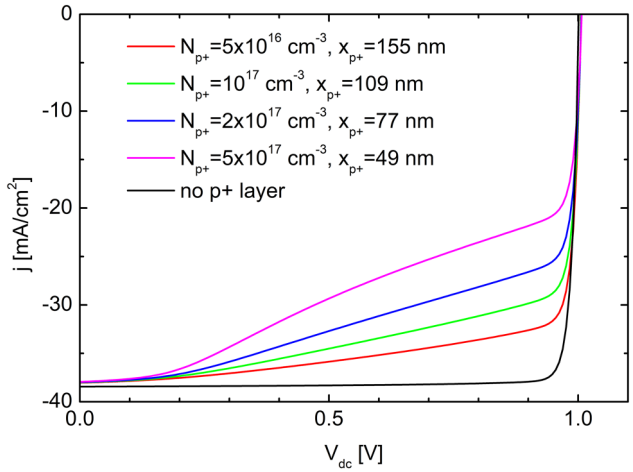

FIG. 10. $j(V_{dc})$ characteristics for structures with different N_{p+} and x_{p+} but exhibiting the same V_{kink} equal to 0.2 V. For comparison, the $j(V_{dc})$ curve corresponding to the structure without the p^+ layer is shown.

On the other hand, the structure with $N_{p+} = 5 \times 10^{16}\,cm^{-3}$ and $x_{p+} = 155$ nm (a red line in Fig. 10) exhibits FF = 79%.

In the case of the same V_{kink}, the shape of the $j(V_{dc})$ curve is determined by the height of the barrier Φ. Using Eqs. (7)–(9), we calculated $\Phi(V_{dc})$ characteristics (Fig. 11). It is visible that a higher N_{p+} results in a higher barrier. This in turn limits the current and decreases the fill factor. Fill factor values corresponding to curves shown in Fig. 10 are collected in Table II.

The relationship between Φ and N_{p+} is quite complicated [Eqs. (7)–(9)]. It can be noticed that Φ rises quite rapidly as a

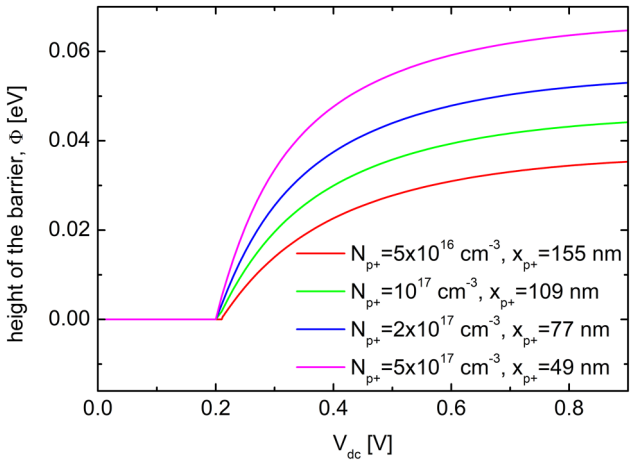

FIG. 11. $\Phi(V_{dc})$ dependences for structures of parameters listed in Table II. Corresponding $j(V_{dc})$ characteristics are presented in Fig. 10.

TABLE II. Parameters of the p^+ layer assumed in simulations shown in Fig. 10. The height of the barrier Φ at $V_{dc} = 0.5$ V was calculated using Eqs. (7)–(9) and the maximal height by Eq. (6). In the case of no p^+ layer, FF = 91.6%. Simulations correspond to T = 150 K.

N_{p+} (cm^{-3})	x_{p+} (nm)	FF (%)	Φ_{max} (eV)	Φ(0.5 V) (eV)
5×10^{16}	155	78.7	0.036	0.028
10^{17}	109	71.6	0.045	0.036
2×10^{17}	77	63.5	0.054	0.044
5×10^{17}	49	52.3	0.066	0.055

function of V_{dc} and its value for $V_{dc} = 0.5$ V is close to its maximal value Φ_{max} (Table II). In all cases, Φ(0.5 V) is about 80% of Φ_{max}. Then, it seems reasonable to focus on the dependence between FF and Φ_{max}. The analysis of Φ_{max} is easier because it is related to N_{p+} with a simple expression [Eq. (6)] and it does not depend on x_{p+}.

The dependence of FF on N_{p+} and Φ_{max} is shown in Fig. 12. Simulations were performed for structures listed in Table II and intermediate cases. In the analyzed range of Φ_{max}, the obtained dependence FF(Φ_{max}) is very close to linear. A similar quasi-linear relationship of FF on Φ(0.5 V) – Φ(0 V) was obtained in Ref. 9. This quasi-linear dependence changes above some Φ and becomes constant, when almost all carriers are blocked and only carriers excited at $x_{max} < x < x_{CIGS}+x_{p+}$ contribute to the photocurrent (not shown here). In that case, our model seems to be insufficient and a correct description of the current should take into account recombination processes.

One of the existing theories explains the p^+ layer by metastable defects, specifically by ($V_{Se} - V_{Cu}$) complexes.[4,11] According to this model, a higher density of the electric charge close to the interface is caused by an increased fraction of ($V_{Se} - V_{Cu}$) complexes in the negative charge state. Simulations of the spatial distribution of charge states of ($V_{Se} - V_{Cu}$) complexes show that x_{p+} should be larger than 200 nm.[9,16,17] A very wide p^+ layer results in reasonable values of V_{kink} only in the case of low acceptor density in the p^+ layer (e.g., $N_{p+} < 5 \times 10^{16}$ cm^{-3}). However, a low N_{p+} would lead to a low Φ and a nonsignificant impact on the fill factor. Hence, an increase in the electric charge probably occurs in a smaller part of the junction than predicted by the standard ($V_{Se} - V_{Cu}$) model. It can be hypothesized that the density of ($V_{Se} - V_{Cu}$) complexes is not constant in the whole absorber. Thus, the nonuniform density of the electric charge is caused not only by a different occupation, but also by a different concentration of metastable defects. A consideration of this possibility may lead to the refinement of the ($V_{Se} - V_{Cu}$) model, in accordance with conclusions of this study.

D. Impact of the temperature and carrier mobility on j (V_{dc}) dependences

Figure 13 shows the results of j(V_{dc}) simulations for structures with different carrier mobilities (μ_e, μ_h) in the p^+ layer corresponding to two temperatures: 150 K and 300 K. Two sets of mobility values were considered: low ($\mu_e = 5$ cm^2/V s, $\mu_h = 2$ cm^2/V s) and high ($\mu_e = 50$ cm^2/V s, $\mu_h = 20$ cm^2/V s). The other parameters were $N_{CIGS} = 3 \times 10^{15}$ cm^{-3}, $N_{p+} = 2 \times 10^{17}$ cm^{-3}, $x_{p+} = 50$ nm, $N_{buf} = 10^{17}$ cm^{-3}, $x_{buf} = 100$ nm, and $\Delta E_V = 0$.

Clearly, the mobility has a strong impact on FF. Its temperature dependence is usually unknown. Therefore, the analysis of the temperature dependence of FF in the presence of the p^+ layer would be a difficult task. However, mobility

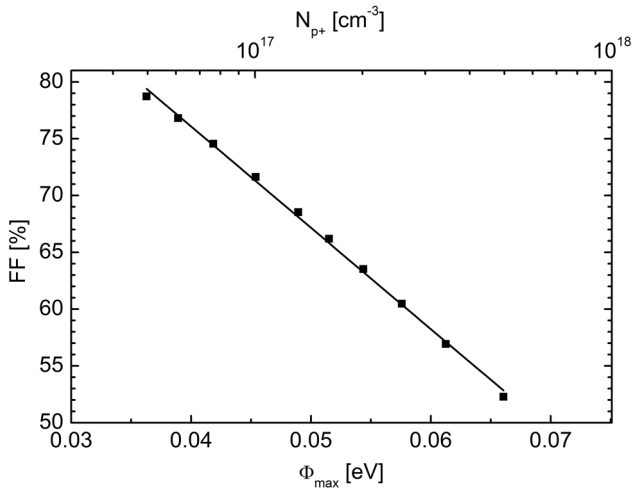

FIG. 12. FF as a function of N_{p+} and Φ_{max} for structures with N_{p+} and x_{p+} resulting in $V_{kink} = 0.2$ V, and with a highly doped buffer (Table II). The dependence of FF on Φ_{max} is similar to linear.

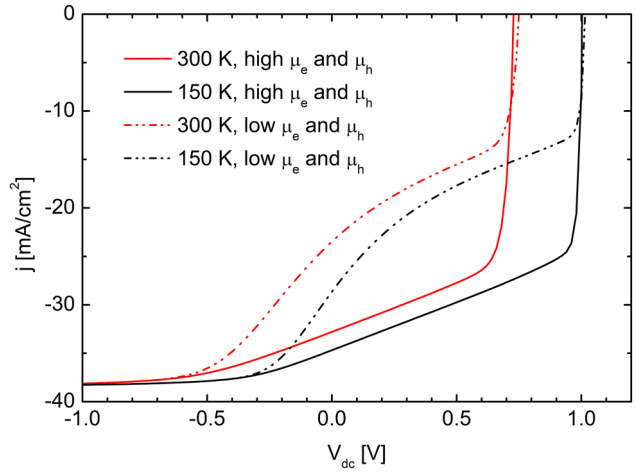

FIG. 13. Simulated j(V_{dc}) dependences corresponding to two temperatures: 150 K (red lines) and 300 K (black lines) and two sets of mobility in the p^+ layer values: $\mu_e = 50$ cm^2/V s, $\mu_h = 20$ cm^2/V s (solid lines) and $\mu_e = 5$ cm^2/V s, $\mu_h = 2$ cm^2/V s (dotted lines).

values have no impact on V_{kink}. Hence, in the analysis of temperature dependences, we should focus on V_{kink}.

Simulations depicted in Fig. 13 suggest that $j(V_{dc})$ characteristics are less affected by the existence of the p^+ layer at lower temperatures. This statement seems to contradict common experimental observations because phenomena typically associated with the p^+ layer (e.g., double diode behavior) are stronger at lower temperatures.[3,5]

The only term in expressions describing V_{kink} depending on the temperature is V_{bi}. Higher temperatures lead to lower V_{bi} and, as a result, lower V_{kink}. It is the origin of the temperature effect depicted in Fig. 13.

This simple understanding neglects other effects that may be responsible for temperature changes of experimental characteristics. Firstly, N_{p+} and x_{p+} may vary with the temperature. Many models link the p^+ layer with metastable defects. At higher temperatures, these defects relax and their occupation may change, which in turn would decrease N_{p+} and x_{p+}. Lower N_{p+} and x_{p+} lead to higher V_{kink} and FF. Furthermore, the carrier density in the buffer layer probably increases with the temperature. Thus, a transition from the lowly to averagely doped buffer cases causes an increase of V_{kink}. Finally, deep levels can hinder the movement of the Fermi level. As a consequence, the temperature dependence of V_{bi} becomes weaker than linear, and thus V_{kink} does not vary significantly at low temperatures. We stress that the change of V_{kink} shown in Fig. 13 corresponds to the case of constant (in terms of temperature) doping of the absorber layer (i.e., no deep levels), which results in approximately linear dependences of the Fermi energy and V_{bi} on the temperature.

IV. CONCLUSIONS

An analytical and numerical study of the model of the p^+ layer was presented. In particular, we focused on its two parameters: the voltage, at which the barrier in the conduction band appears (V_{kink}), and the height of the barrier (Φ). Our goal was to relate these quantities with parameters of the p^+ layer, like its width or density of acceptors.

The usefulness of V_{kink} comes from the fact that it can be easily read from $j(V_{dc})$ characteristics as a V_{dc}, at which the deterioration of the curve begins. Equations relating V_{kink} with the width and density of acceptors in the p^+ layer were derived [Eqs. (2)–(4)]. Three final expressions correspond to three possible distributions of the electric potential in the buffer layer. Usually, the highest values of V_{kink} [the weakest deterioration of the $j(V_{dc})$ curve] are obtained for the highly doped buffer. In the case of lowly doped buffer, V_{kink} decreases with the width of the buffer layer.

In the second step, we analyzed how the height of the barrier Φ depends on the applied voltage V_{dc}. The derived formulas are quite complicated [Eqs. (7)–(9)], but the analysis allowed for pointing out a simple expression for the maximal value of Φ, achieved at high V_{dc} [Eq. (6)]. Φ_{max} increases with N_{p+} and is independent from x_{p+}.

Examples of analyses employing derived expressions were shown. Based on V_{kink} and using Eqs. (2) and (4), it is possible to determine the upper and lower limits of the density of acceptors in the p^+ layer. By analyzing the impact of Φ on the fill factor of $j(V_{dc})$ curves exhibiting equal V_{kink}, we found almost a linear relationship between FF and Φ_{max} (or the logarithm of the density of acceptors in the p^+ layer). Moreover, we noticed that the impact of the p^+ layer should be more significant (lower V_{kink}) at higher temperatures. However, our model does not take into account temperature dependences of parameters of the p^+ or buffer layers as well as a possible impact of deep levels.

Finally, it was concluded that the uniform distribution of $(V_{Se} - V_{Cu})$ metastable complexes should result in a wide but relatively lowly doped p^+ layer, whose effect on the fill factor is weak. It was concluded that an assumption of a nonuniform distribution of metastable defects may lead to a better accordance of the $(V_{Se} - V_{Cu})$ model with experimental observations.

ACKNOWLEDGMENTS

The author acknowledges the critical reading of the manuscript by Dr. Pawel Zabierowski (Warsaw University of Technology) and Professor Jennifer Heath (Linfield College) and their valuable comments.

APPENDIX A: DERIVATION OF V_{KINK}

By analyzing the appearance of the barrier, the hole density in the p^+ layer can be neglected. The electric charge of holes becomes more relevant only for V_{dc} substantially more than V_{kink}, when the VBM at $x_{CIGS} < x < x_{max}$ becomes close to the Fermi level, and the hole density becomes comparable to N_{p+}. We stress that holes in the standard CIGS (for $0 < x < x_{CIGS}$) cannot be neglected because in this region in the presence of the barrier the hole concentration (p) is larger than N_{CIGS}.

In our calculations, we put $\varphi(x = 0) = 0$. As it was told, $x = 0$ represents the edge of the space charge region in the standard CIGS. If $\Phi > 0$ (i.e., the barrier exists) and energy bands in the standard CIGS rise, $\varphi(x)$ falls and its values are negative.

In the first step, we derive the relationship between $\varphi(x_{CIGS})$ and $E(x_{CIGS})$. Assuming the constant position of the hole quasi-Fermi energy (E_{Fp}), the hole density is

$$p = N_V \exp\frac{E_V - E_{Fp}}{k_B T} = N_V \exp\frac{E_V(x=0) - e\varphi - E_{Fp}}{k_B T} = N_{CIGS} \exp\frac{-e\varphi}{k_B T}, \tag{A1}$$

where E_V stands for the energy of the VBM. Using the identity $\frac{d^2\varphi}{dx^2} = -\frac{dE}{dx} = \frac{dE}{d\varphi}E$ and Eq. (A1), we obtain the formula linking the electric field and the electric potential at the edge of the standard CIGS,

$$E(x_{CIGS}) = \pm\sqrt{\frac{2eN_{CIGS}}{\varepsilon_0\varepsilon_1}\left[\varphi(x_{CIGS}) + \frac{k_B T}{e}\left(\exp\frac{-e\varphi(x_{CIGS})}{k_B T} - 1\right)\right]}. \tag{A2}$$

This formula will be used in further analyses. The sign of $E(x_{CIGS})$ depends on the spatial dependence of the electric potential. In the standard situation, energy bands go down with x, so the electric field is negative and $E(x_{CIGS}) < 0$. On the other hand, if the electric charge in CIGS is positive ($e_p > eN_{CIGS}$), the electric field is positive. This case corresponds to rising energy bands and the appearance of the barrier. In this situation, $E(x_{CIGS}) > 0$.

It should be noticed that in the whole standard CIGS (i.e., $0 < x < x_{CIGS}$), the electric charge is either positive (energy bands rise) or negative (energy bands fall). As a result, the electric field in the standard CIGS changes monotonically—either rises ($\Phi > 0$) or falls (no barrier). Hence, E(x) does not change its sign and the electric potential does not achieve neither minimum nor maximum for $0 < x < x_{CIGS}$.

Our objective is to find the value of the applied voltage, for which the barrier appears. We denote this value of V_{dc} as V_{kink}. If the barrier is low ($\Phi \approx 0$), holes in the p^+ layer can be neglected. Hence,

$$\frac{d^2\varphi}{dx^2} = \frac{eN_{p+}}{\varepsilon_0\varepsilon_1} \tag{A3}$$

for $x_{CIGS} < x < x_{CIGS} + x_{p+}$. In the next step, we obtain

$$E(x) = E(x_{CIGS}) - \frac{eN_{p+}}{\varepsilon_0\varepsilon_1}(x - x_{CIGS}). \tag{A4}$$

In the standard case (no barrier), the electric field in the p^+ layer is always negative. The barrier exists when the electric potential exhibits minimum in the p^+ layer. The minimum of φ corresponds to $E(x) = 0$. Hence, the barrier exists if E(x) changes the sign in the p^+ layer. This condition can be fulfilled only if $E(x_{CIGS}) > 0$. On the other hand, if $E(x_{CIGS}) < 0$, the electric field does not change the sign (no barrier). Clearly, $E(x_{CIGS}) = 0$ implies that $\varphi(x_{CIGS}) = 0$ [cf. Eq. (A2)].

Further calculations lead from Eq. (A4) to

$$\varphi(x_{CIGS} + x_{p+}) = \varphi(x_{CIGS}) + \frac{eN_{p+}x_{p+}^2}{2\varepsilon_0\varepsilon_1} - x_{p+}E(x_{CIGS}). \tag{A5}$$

The barrier appears, when $E(x_{CIGS})$ and $\varphi(x_{CIGS})$ change the sign and become positive and negative, respectively. The limit value of the V_{dc} corresponds to $E(x_{CIGS}) = \varphi(x_{CIGS}) = 0$. As a result,

$$\varphi(x_{CIGS} + x_{p+}) = \frac{eN_{p+}x_{p+}^2}{2\varepsilon_0\varepsilon_1}. \tag{A6}$$

The relationship between V_{kink} and properties of the p^+ layer (N_{p+}, x_{p+}) depends on $\varphi(x_{CIGS} + x_{p+})$, which is determined by the distribution of the electric potential in the buffer layer.

In the case of high density of donors in the buffer layer (N_{buf}), bands in the buffer layer are flat, and the Fermi level achieves the CBM at the p^+/buffer interface. As a result, $\varphi(x_{CIGS} + x_{p+}) = V_{bi} - V_{dc}$, and Eq. (2).

As an "averagely doped buffer layer," we understand the situation when the thickness of the buffer layer (x_{buf}) is larger than its depletion width (x_{bSCR}). In this case, we solve Eq. (1c). It leads to

$$\varphi(x_{CIGS} + x_{p+}) = V_{bi} - V_{dc} - \frac{eN_{buf}x_{bSCR}^2}{2\varepsilon_0\varepsilon_2}. \tag{A7}$$

The space charge neutrality condition imposes that $Q_{CIGS} - eN_{p+}x_{p+} + eN_{buf}x_{bSCR} = 0$, where Q_{CIGS} is a total space charge in the standard CIGS. Q_{CIGS} can be simply calculated from the Gauss law: $Q_{CIGS} = E(x_{CIGS})\epsilon_0\epsilon_1$. As we explained, the barrier appears (in other words: $V_{dc} = V_{kink}$) if $E(x_{CIGS}) = 0$. It leads to $N_{p+}x_{p+} = N_{buf}x_{bSCR}$. From this equality, we obtain Eq. (3).

If N_{buf} is small ("lowly doped buffer layer," case c in Sec. II), the buffer layer is depleted in its whole thickness. As the doping level of the window layer is assumed high, $\varphi(x_{CIGS} + x_{p+} + x_{buf}) = V_{bi} - V_{dc}$. It should be noted that $E(x_{CIGS} + x_{p+} + x_{buf}) \neq 0$. The solution of Eq. (1c) leads to Eq. (4).

How could we distinguish situations of "averagely" and "lowly doped buffer layer"? Firstly, it should be noticed that x_{bSCR} depends on V_{dc}, and the increase of V_{dc} can switch from $x_{bSCR} > x_{buf}$ to $x_{bSCR} < x_{buf}$. Equations (3) and (4) were derived for x_{bSCR} corresponding to $V_{dc} = V_{kink}$. Hence, the adequate condition should be found based on the relationship between $x_{bSCR}(V_{dc} = V_{kink})$ and x_{buf}. As it was shown previously, if $V_{dc} = V_{kink}$, $E(x_{CIGS}) = 0$. Hence, $V_{dc} = V_{kink}$ and $x_{bSCR} < x_{buf}$ lead to $N_{p+}x_{p+} = N_{buf}x_{bSCR}$. This equality is a base of the distinction between these two regimes: if $N_{p+}x_{p+} < N_{buf}x_{buf}$, the buffer layer is depleted only partially and Eq. (3) is adequate. Otherwise, the buffer is completely depleted, and Eq. (4) correctly describes V_{kink}. It is important that the obtained condition depends on the width of the buffer layer (x_{buf}) but not on the depletion width in the buffer layer (x_{bSCR}).

APPENDIX B: Φ IN THE CASE OF NONZERO VALENCE BAND

To take into account the valence band offset, we express hole concentration in the p^+ layer as

$$\begin{aligned} p &= N_V \exp\frac{E_V(x=0) - e\varphi - \Delta E_V - E_{Fp}}{k_B T} \\ &= N_{CIGS} \exp\frac{-e\varphi - \Delta E_V}{k_B T}. \end{aligned} \tag{B1}$$

In this case, E in the p^+ layer is

$$\begin{aligned} E^2(\varphi) = \frac{2eN_{CIGS}}{\varepsilon_0\varepsilon_1}\Bigg[&\varphi(x_{CIGS}) + \frac{k_B T}{e}\left(\exp\frac{-e\varphi(x_{CIGS})}{k_B T} - 1\right) \\ &+ \frac{k_B T}{e}\exp\frac{-\Delta E_V}{k_B T}\left(\exp\frac{-e\varphi}{k_B T} - \exp\frac{-e\varphi(x_{CIGS})}{k_B T}\right)\Bigg] \\ &+ \frac{2eN_{p+}}{\varepsilon_0\varepsilon_1}[\varphi - \varphi(x_{CIGS})]. \end{aligned} \tag{B2}$$

Moreover, the other expression for the hole concentration imposes modification in the relationship between $\varphi(x_{CIGS})$ and $\varphi(x_{max})$. It is not possible to give a direct expression for $\varphi(x_{CIGS})$, however. Putting $E^2[\varphi(x_{max})] = 0$ leads to

$$N_{CIGS}\left[\varphi(x_{CIGS}) + \frac{k_BT}{e}\left(\exp\frac{-e\varphi(x_{CIGS})}{k_BT} - 1\right) + \frac{k_BT}{e}\exp\frac{-\Delta E_V}{k_BT}\left(\exp\frac{-e\varphi(x_{max})}{k_BT} - \exp\frac{-e\varphi(x_{CIGS})}{k_BT}\right)\right] + N_{p+}[\varphi(x_{max}) - \varphi(x_{CIGS})] = 0. \quad \text{(B3)}$$

To find $\varphi(x_{CIGS})$ for given $\varphi(x_{max})$, Eq. (B3) should be solved numerically. The height of the barrier can be calculated by solving Eq. (8) with Eq. (B3). As $E(\varphi)$ in Eq. (8), expression from Eq. (B2) should be taken.

Lower E_V leads to lower hole concentration in the p^+ layer. Hence, in the case of large ΔE_V, it could be expected that the neglection of holes in the p^+ layer could give results close to accurate [Eqs. (8) and (B3)]. To find $\varphi(x_{max})$ neglecting holes in the p^+ layer, we base on Eq. (A3). Using Eq. (A4) and knowing that $E(x_{max}) = 0$, we obtain

$$x_{max} = x_{CIGS} + \frac{\varepsilon_0\varepsilon_1 E(x_{CIGS})}{eN_{p+}}. \quad \text{(B4)}$$

The electric potential can be obtained by the integration of Eq. (A4). The potential at $x = x_{max}$ is

$$\varphi(x_{max}) = \varphi(x_{CIGS}) - \frac{N_{CIGS}}{N_{p+}}\left[\varphi(x_{CIGS}) + \frac{k_BT}{e}\left(\exp\frac{-e\varphi(x_{CIGS})}{k_BT} - 1\right)\right]. \quad \text{(B5)}$$

In the case of highly doped buffer, Eq. (A5) can be rewritten by making use of Eq. (A2),

$$V_{bi} - V_{dc} = \varphi(x_{CIGS}) + \frac{eN_{p+}x_{p+}^2}{2\varepsilon_0\varepsilon_1} - x_{p+}\sqrt{\frac{2eN_{CIGS}}{\varepsilon_0\varepsilon_1}\left[\varphi(x_{CIGS}) + \frac{k_BT}{e}\left(\exp\frac{-e\varphi(x_{CIGS})}{k_BT} - 1\right)\right]}. \quad \text{(B6)}$$

Solving Eqs. (B5) and (B6), $\Phi = -e\varphi(x_{max})$ can be found. Hence, this method allows for the calculation of Φ in the absence of holes in the p^+ layer.

APPENDIX C: PARAMETERS USED IN SIMULATIONS

Left and right contacts surface recombination velocity: 10^7 cm/s (for electrons and holes)

	Cu(In,Ga)Se_2	p^+	Buffer	Window
Thickness (μm)	2.5	[a]	[a]	0.2
Bandgap (eV)	1.2	1.2[b]	2.45	3.4
Dielectric constant	12	12	10	10
Electron affinity (eV)	4.5	4.5	4.5	4.5
Effective density of states in CB (300 K) (cm^{-3})	7×10^{17}	7×10^{17}	3×10^{18} [c]	4×10^{18}
Effective density of states in VB (300 K) (cm^{-3})	1.8×10^{19}	1.8×10^{19}	1.5×10^{19}	9×10^{18}
Electron mobility (cm^2/V s)	50	50[b]	50	50
Hole mobility (cm^2/V s)	20	20[b]	20	20

[a]Values given in the paper for every simulation.
[b]If not stated otherwise.
[c]In the case of high N_{buf} (like in Sec. III C), this value was increased.

REFERENCES

[1]D. Schmid, M. Ruckh, F. Grunwald, and H. Schock, J. Appl. Phys. **73**, 2902 (1993).
[2]M. Igalson, M. Bodegard, and L. Stolt, Sol. Energy Mater. Sol. Cells **80**, 195 (2003).
[3]M. Igalson, A. Urbaniak, P. Zabierowski, H. Abdel-Maksoud, M. Buffiere, N. Barreau, and S. Spiering, Thin Solid Films **535**, 302 (2013).
[4]M. Igalson, P. Zabierowski, D. Przado, A. Urbaniak, M. Edoff, and W. N. Shafarman, Sol. Energy Mater. Sol. Cells **93**, 1290 (2009).
[5]M. Richter, C. Schubbert, P. Eraerds, J. Parisi, I. Riedel, T. Dalibor, and J. Palm, Sol. Energy Mater. Sol. Cells **132**, 162 (2015).
[6]M. Nichterwitz, R. Caballero, C. A. Kaufmann, H.-W. Schock, and T. Unold, J. Appl. Phys. **113**, 044515 (2013).
[7]U. Rau and H. W. Schock, in *Practical Handbook of Photovoltaics: Fundamentals and Applications*, edited by A. McEvoy, T. Markvart, and L. Castaner (Elsevier, 2003).
[8]A. Niemegeers, M. Burgelman, R. Herberholz, U. Rau, D. Hariskos, and H.-W. Schock, Prog. Photovolt. Res. Appl. **6**, 407 (1998).
[9]M. Burgelman, K. Decock, S. Khelifi, and A. Abass, Thin Solid Films **535**, 296 (2013).
[10]P. Zabierowski, in *Thin Film Solar Cells: Current Status and Future Trends*, edited by A. Bosio and A. Romeo (Nova Science Publishers, Inc., 2010).
[11]S. Lany and A. Zunger, J. Appl. Phys. **100**, 113725 (2006).
[12]S. Lany and A. Zunger, Phys. Rev. Lett. **100**, 016401 (2008).
[13]M. Burgelman, P. Nollet, and S. Degrave, Thin Solid Films **361–362**, 527 (2000).
[14]J. Pettersson, C. Platzer-Bjorkman, A. Hultqvist, U. Zimmermann, and M. Edoff, Phys. Scr. **T141**, 014010 (2010).
[15]S. Ishizuka, J. Nishinaga, M. Iioka, H. Higuchi, Y. Kamikawa, T. Koida, H. Shibata, and P. Fons, Adv. Energy Mater. **8**, 1702391 (2018).
[16]K. Decock, P. Zabierowski, and M. Burgelman, J. Appl. Phys. **111**, 043703 (2012).
[17]M. Maciaszek and P. Zabierowski, IEEE J. Photovoltaics **5**, 1454 (2015).